Published in final edited form as:

Hepatology. 2018 November ; 68(5): 1991–2003. doi:10.1002/hep.30070.

Excessive plasmin compromises hepatic sinusoidal vascular integrity after acetaminophen overdose

Siqi Gao[1,2], **Robert Silasi-Mansat**[1], **Mandi Behar**[1], **Florea Lupu**[1,2], and **Courtney T. Griffin**[1,2]

[1]Cardiovascular Biology Research Program, Oklahoma Medical Research Foundation, Oklahoma City, OK

[2]Department of Cell Biology, University of Oklahoma Health Sciences Center, Oklahoma City, OK

Abstract

The serine protease plasmin degrades extracellular matrix (ECM) components both directly and indirectly through activation of matrix metalloproteinases. Excessive plasmin activity and subsequent ECM degradation causes hepatic sinusoidal fragility and hemorrhage in developing embryos. We report here that excessive plasmin activity in a murine acetaminophen (APAP) overdose model likewise compromises hepatic sinusoidal vascular integrity in adult animals. We found that hepatic plasmin activity is upregulated significantly at 6 hr after APAP overdose. This plasmin upregulation precedes both degradation of the ECM component fibronectin around liver vasculature and bleeding from centrilobular sinusoids. Importantly, administration of the pharmacological plasmin inhibitor tranexamic acid or genetic reduction of plasminogen, the circulating zymogen of plasmin, ameliorates APAP-induced hepatic fibronectin degradation and sinusoidal bleeding. *Conclusion:* These studies demonstrate that reduction of plasmin stabilizes hepatic sinusoidal vascular integrity after APAP overdose.

Keywords

APAP; fibronectin; tranexamic acid; plasminogen; centrilobular bleeding

Introduction

The circulating zymogen plasminogen, which is primarily synthesized in the liver, is converted to the serine protease plasmin by widely expressed plasminogen activators(1). Plasmin is a potent thrombolytic protease that dissolves fibrin blood clots and targets extracellular matrix (ECM) components for degradation. It directly cleaves some ECM components, such as laminin and fibronectin, and it indirectly cleaves additional ECM components by activating matrix metalloproteinases (MMPs)(2, 3).

We previously reported that excessive plasmin activation and subsequent ECM degradation causes embryonic vascular fragility (4, 5). Embryonic hepatic sinusoidal blood vessels are particularly prone to rupture when their underlying laminin-rich ECM is degraded by

Contact Information: Courtney T. Griffin; Oklahoma Medical Research Foundation, 825 NE 13th Street, Oklahoma City, OK, 73104; phone: 405-271-7073; fax: 405-271-3137; courtney-griffin@omrf.org.

plasmin(5). However, since laminin is downregulated in perisinusoidal spaces after birth(6), it is unclear whether excessive plasmin activity can cause vascular fragility in an adult liver.

Acetaminophen (APAP) overdose is the leading cause of drug-induced liver injury in the United States(7). In addition to centrilobular hepatocyte necrosis, APAP overdose also causes centrilobular bleeding(8), and some reports indicate that vascular damage precedes hepatocyte damage in mouse models of APAP overdose(9, 10). Intriguingly, plasmin activation exacerbates APAP-induced hepatic injury in mice. Increased plasmin activation through administration of recombinant tissue plasminogen activator elevates APAP-induced liver injury and bleeding in wildtype mice(11). Conversely, both pharmacological plasmin inhibition and genetic deletion of plasminogen reduce hepatic damage and bleeding after APAP overdose(11). Moreover, mice with genetic deletion of the plasminogen activator inhibitor PAI-1, which presumably have excessive plasmin activity, suffer massive intrahepatic bleeding after APAP overdose(11, 12). Altogether, these published data suggest a causative relationship between plasmin activation and hepatic vascular damage following APAP overdose. However, a systematic and mechanistic analysis of this putative relationship is missing from the literature and therefore is the subject of this study.

Materials and Methods

Mice

Eight to ten week old male C57Bl/6J mice from Jackson Laboratories (Bar Harbor, ME) with an average weight of 25 g were used in this study. Mice were socially housed in autoclaved ventilated microisolator cages with autoclaved corn cob bedding and mouse igloos from Bio-Serv (Flemington, NJ) for enrichment in a room with a 14/10-hour light/dark cycle. They were provided chlorinated reverse osmosis water delivered in pouches and irradiated PicoLab Rodent Diet 20 (Cat. #5053) from LabDiet (St. Louis, MO). Mice were fasted for approximately 16 hr (overnight) prior to treatment with 300 mg/kg APAP (Cat. #A5000; Sigma-Aldrich, St. Louis, MO) dissolved in warm sterile saline solution (Cat. #0409-7983-61; Hospira, Lake Forest, IL) and delivered via intraperitoneal injection. Food was returned immediately after treatment with APAP or vehicle. When indicated, mice were additionally treated with 600 mg/kg tranexamic acid (TA; Spectrum Chemicals & Laboratory Products, New Brunswick, NJ) delivered via intraperitoneal injection at 2 hr after APAP overdose. Eight to eleven week old male littermate wildtype ($Plg^{+/+}$) and plasminogen-deficient ($Plg^{+/-}$, $Plg^{-/-}$) mice on a C57Bl/6J background were used for genetic studies and were housed together prior to and during the experiments. Plasminogen-deficient mice(13) were genotyped by PCR (65°C annealing temperature) using a forward primer (5'-AATCCCAAGCTGAGTAAAGACAGTGG-3') and a reverse primer (5'-TTAGGTAATGGAGACACGGAGGTGTT-3'), which produce a 256 bp amplicon from a wildtype *Plg* allele, in combination with a forward primer (5'-GACATGGATGGCTGAACCGTCTCTGT-3') and a reverse primer (5'-ACAAGCAAAACCAAATTAAGGGCCA-3'), which produce a 495 bp amplicon from a knockout *Plg* allele. All experimental animal protocols were approved by the Institutional Animal Care and Use Committee at the Oklahoma Medical Research Foundation.

Hepatotoxicity assessment

300 μl of blood was drawn from the heart immediately after euthanasia and centrifuged at 7,000 g for 5 min at 20°C. Serum was collected and subjected to alanine aminotransferase (ALT) measurement using a Catalyst One Chemistry Analyzer from IDEXX Laboratories, Inc. (Westbrook, ME).

Histological staining

Prior to euthanasia, anesthetized animals were perfused with PBS and then perfused with 4% paraformaldehyde at a rate of 5 mL/min using a 101U/R peristaltic pump from Watson-Marlow Fluid Technology Group (Wilmington, MA). Median liver lobes were subjected to additional immersion fixation in 4% paraformaldehyde overnight and embedded in paraffin blocks. Liver samples from $Plg^{+/+}$, $Plg^{+/-}$, and $Plg^{-/-}$ mice were collected without perfusion but were immersion fixed in 4% paraformaldehyde overnight prior to embedding; we did not see dramatic differences in histological blood detection using this technique versus perfusion fixation. Histological sections were cut at 7μm thickness using an HM 355S microtome from Microm International (Walldorf, Germany). Setions were mounted on UltraClear Microscope slides from Denville Scientific Inc. (Holliston, MA) and allowed to dry overnight prior to hematoxylin and eosin staining, which was performed as described(14). The extent of sinusoidal hemorrhage was determined by measuring the hemorrhage area relative to the entire histological section after rendering red blood cells to black and other cells to white using Fiji software(15).

Microscopy and image acquisition

Brightfield histological images were obtained with an Eclipse 80i microscope from Nikon (Melville, NY) using 4× (NA 0.13) and 20× (NA 0.5) objectives and a Nikon DS-Fi1 camera. Fluorescence images were obtained with a Nikon Eclipse Ti-E inverted microscope using a 40× (NA 0.6) objective, an Andor Zyla 4.2 camera, and an X-cite 120LED light source. NIS-Elements AR3.0 (Nikon) software was used for brightfield image acquisition and assembly, and NIS-Elements AR4.6 (Nikon) software was used for fluorescence image acquisition and assembly.

Plasmin activity assay

100 mg of total liver was homogenized in RIPA buffer (50 mM Tris, 1% Triton X-100, 1.1% sodium deoxycholate, 0.1% SDS, and 150 mM NaCl) without protease inhibitors. Lysates were centrifuged at 15,000 g for 15 min at 4°C. The supernatant was collected and analyzed for plasmin activity. Protein concentration was determined using the Pierce BCA Protein Assay Kit and a NanoDrop 2000 from Thermo Fisher Scientific (Waltham, MA). Plasmin activity was measured using 0.1 mmol/L of a plasmin-specific fluorogenic substrate Boc-Glu-Lys-Lys-MCA (Cat. #MEK-3105-v) from Peptides International Inc. (Louisville, KY). Flourescence from the liver homogenate was compared against a standard curve generated with human plasmin (Cat. #P1867; Sigma-Aldrich). A FLUOstar Omega microplate reader (excitation 355 nm; emission 460 nm) from BMG LABTECH (Ortenberg, Germany) was used for measuring fluorescence.

In situ zymography

The upper half of left liver lobes was cryosectioned without prior fixation. Sections (12μm) were overlaid with in situ zymography solution consisting of 1% UltraPure low melting point agarose (Thermo Fisher Scientific), 10 mmol/L Boc-Glu-Lys-Lys-MCA or 1mg/ml quenched BODIPY FL casein from the EnzChek Protease Assay Kit (Thermo Fisher Scientific). Overlaid sections were coverslipped and incubated for 30 minutes at 37°C. Substrate cleavage was detected by fluorescence microscopy.

Immunoblot

Liver tissue (100 mg) was homogenized in RIPA buffer with Protease Inhibitor Cocktail (Cat. # P8340; Thermo Fisher Scientific). Lysates were centrifuged at 10,000 g for 15 min at 4°C. The supernatant was collected and analyzed. Protein concentration was determined as above described for the plasmin activity assay. Plasminogen from human plasma (Sigma-Aldrich) was used as a positive control sample for plasminogen/plasmin detection. Protein (30 μg) was electrophoresed on a 9% SDS-PAGE gel and then transferred to a PVDF membrane that was blocked in 5% nonfat dry milk-TBST for 1 hr. Primary antibodies (diluted in 5% milk-TBST) were incubated at 4°C overnight with gentle agitation, and membranes were then washed three times (10 min each) in TBST. HRP-conjugated secondary antibodies (diluted in 5% milk-TBST) were applied at room temperature for 1 hr with gentle agitation, and membranes were then washed five times (15 min each) in TBST. Secondary antibodies were detected using ECL Western Blotting Detection Reagents (Cat. #RPN2209) from GE Healthcare (Chicago, IL). Primary antibodies used for immunoblotting: Plasminogen/Plasmin (1:1000, #AMPG-9130) from Haematologic Technologies (Essex Junction, VT), Fibronectin (1:1000, #Ab2413) from Abcam (Cambridge, United Kingdom), GAPDH (1:10000, #G9545) from Sigma-Aldrich.

Real-time quantitative PCR (qPCR)

Total RNA was extracted from 100 mg of liver samples using the RNeasy Mini kit (#74106) from Qiagen (Germantown, MD). cDNA was prepared using the iSCRIPT™ Reverse Transcriptase Kit from Bio-Rad (Hercules, CA), and qPCR was performed using 2× SYBR green qPCR master mix (Thermo Fisher Scientific) and the CFX96 Real-Time System (Bio-Rad) with gene-specific primers (Supplemental Table. 1).

Transmission electron microscopy (TEM) and scanning electron microscopy (SEM)

Prior to euthanasia, anesthetized animals were perfused with PBS and then perfused with fixative (2.5% glutaraldehyde and 2% paraformaldehyde in 0.1 M sodium cacodylate buffer) at a rate of 5 mL/min using a 101U/R peristaltic pump from Watson-Marlow Fluid Technology Group (Wilmington, MA). For TEM, liver samples were further fixed by immersion in the same fixative for 1 hr, followed by post-fixation in 1% osmium tetroxide (90 min) and 1% tannic acid (1 hr). Samples were subsequently dehydrated in a graded ethanol series and embedded in epoxy resin from Electron Microscopy Sciences (Hatfield, PA). Ultrathin sections (70 nm) were cut using an EM UC7 ultramicrotome from Leica (Wetzlar, Germany) equipped with a diamond knife. Sections were stained with uranyl acetate and lead citrate before being viewed with an H-7600 electron microscope from

Hitachi (Tokyo, Japan) equipped with a 4 megapixel digital monochrome camera and AMT-EM image acquisition software from Advanced Microscopy Techniques (Woburn, MA). For SEM, liver tissue pieces were excised after perfusion fixation and were further fixed by immersion in the same fixative overnight. Liver tissue was then sliced into 1 mm thick sections with a vibratome, washed with sodium cacodylate buffer, and then post-fixed with 1% osmium tetroxide in 0.1 M cacodylate buffer for 90 min. After washing with cacodylate buffer, tissue slices were dehydrated in a graded ethanol series. The sections were further dehydrated in hexamethyldisilazane (HMDS) and allowed to air-dry overnight. Tissue sections were then sputter-coated with Au/Pd particles using a Med-010 Sputter Coater from Balzers (Schaumburg, IL) and imaged with a Quanta 600 SEM from FEI (Hillsboro, OR) at an accelerating voltage of 20KV.

Immunofluorescence

The lower half of left liver lobes was cryosectioned without prior fixation. Sections (7 μm) were taken from the freezer before staining, and warmed at room temperature for 3 min. Sections were fixed with 4% paraformaldehyde for 15 min and permeabilized with 0.1% Triton X-100 for 15 min at room temperature, washed three times (5 min each) with PBS, then blocked in blocking solution (5% normal goat serum/5% normal donkey serum/0.3% BSA/0.1% Triton X-100 in PBS) for 1 hr at room temperature. Sections were incubated in primary antibody diluted in blocking solution overnight at 4°C, washed three times (3 min each) with PBS, then incubated for 1 hr at room temperature in secondary antibody at a 1:500 concentration in blocking solution along with 10 μg/ml Hoechst stain (Cat. # 89139-124) from VWR International (Irving, TX). Primary antibodies used for immunofluorescence: Fibronectin (1:100, #Ab2413; Abcam), Collagen I (1:100, #Ab34710; Abcam), Collagen IV (1:100, #Ab6586; Abcam), Laminin (1:100, #Ab11575; Abcam), Cytokeratin 19 (1:1, Clone: TROMA-III) from Developmental Studies Hydridoma Bank (Iowa City, IA).

Results

APAP-induced hepatic sinusoidal bleeding is plasmin dependent

Administration of 300 mg/kg APAP to 8–10 week old C57Bl/6J male mice following 16 hr of fasting causes increasing centrilobular hepatocyte necrosis (Fig. 1A) and elevated serum alanine aminotransferase (ALT) measurements (Supplemental Fig. 1A) over 24 hr. Bleeding likewise occurs from centrilobular sinusoidal blood vessels by 6 hr after APAP overdose, and it increases in severity by 24 hr (Fig. 1A). Since plasmin contributes to APAP-induced hepatic injury(11, 12) and to embryonic hepatic sinusoidal fragility(5), we sought to test the role of plasmin in APAP-induced hepatic bleeding. We first used the pharmacological plasmin inhibitor tranexamic acid (TA), which we administered 2 hr after APAP overdose. In our hands, TA treatment did not alter serum ALT levels measured 24 hr after APAP overdose (Supplemental Fig. 1B). However, centrilobular sinusoidal bleeding at 24 hr after APAP overdose was significantly diminished in TA-treated animals (Fig. 1B). We also took a genetic approach to reduce plasmin in the APAP overdose model by using male mice deficient for the plasmin zymogen, plasminogen ($Plg^{+/-}$ and $Plg^{-/-}$). Once again, we saw no alteration in serum ALT levels at 24 hr after APAP treatment between littermate wildtype

(WT) and *Plg*$^{+/-}$ or *Plg*$^{-/-}$ mice (Supplemental Fig. 1C). However, as with TA treatment, centrilobular sinusoidal hemorrhage was significantly reduced in *Plg*$^{+/-}$ and *Plg*$^{-/-}$ mice versus WT littermates at 24 hr after APAP overdose (Fig. 1C). These pharmacological and genetic data indicate that plasmin contributes to APAP-induced sinusoidal hemorrhage.

Plasmin activity is elevated by 6 hr after APAP overdose

In order to determine the level of plasmin activity following APAP overdose, we used a synthetic plasmin substrate that fluoresces upon cleavage(16). With this substrate, we found plasmin activity to be significantly and specifically elevated 6 hr after APAP overdose in whole liver lysates (Fig. 2A). Notably, this corresponds to the time point at which we see centrilobular sinusoidal bleeding beginning to accumulate after APAP overdose (Fig. 1A). When used for in situ zymography analysis on fresh liver sections, this same synthetic plasmin substrate likewise revealed increased plasmin activity surrounding blood vessels at 6 hr after APAP overdose (Figure 2B). Immunoblotting of liver lysates with an antibody that recognizes both plasminogen and plasmin confirmed that plasmin is elevated at 6 hr after APAP overdose (Fig. 2C).

Plasmin is activated from its circulating zymogen plasminogen by tissue plasminogen activator (tPA) or by the urokinase plasminogen activator (uPA) and its receptor (uPAR). In order to address whether expression of plasminogen or the plasminogen activators was impacted by APAP overdose, we performed qPCR on total liver samples. We found *tPA* to be significantly upregulated by 4 hr after APAP overdose (Fig. 2D), which precedes the 6 hr time point at which our multiple assays showed elevated plasmin activity (Fig. 2A–C). Therefore, an APAP-mediated increase in hepatic *tPA* expression may contribute to the elevated plasmin activity seen 6 hr after APAP overdose.

Sinusoidal endothelial cells have cavernous gaps by 6 hr after APAP overdose

To assess sinusoidal endothelial cell morphology at the time of peak APAP-induced plasmin elevation and at the start of APAP-induced sinusoidal bleeding, we processed liver samples for transmission electron microscopy (TEM) and scanning electron microscopy (SEM) at 6 hr after APAP overdose. We observed relatively normal sinusoidal endothelial cell morphology at 6 hr after APAP overdose by TEM, unlike the surrounding hepatocytes that showed evidence of necrosis, including swollen organelles and extreme vacuolization (Fig. 3A). However, we did notice a consistent increase in sinusoidal diameter (Supplemental Fig. 2A, B) and in the space of Disse between sinusoids and hepatocytes (Supplemental Fig. 2A, C) at 6 hr after APAP overdose by TEM. Interestingly, TA treatment did not ameliorate APAP-induced dilation in sinusoids or the space of Disse after APAP overdose (Supplemental Fig. 2). We also saw small fenestrations and larger gaps in sinusoidal endothelial surfaces by SEM after saline and APAP treatments (Fig. 3B). However, the larger gaps appeared more cavernous with less underlying meshwork—which may represent extracellular matrix (ECM)—and were seen near extravascular red blood cells after APAP treatment. Additional TA treatment eliminated the extravascular red blood cells and restored some of the meshwork under the larger gaps in the endothelial cell surfaces, although the space of Disse was still visibly enlarged. Altogether, these electron microscopy data indicate that dilated sinusoids and an expanded space of Disse are not plasmin dependent and do not

contribute to APAP-induced sinusoidal bleeding. However, large endothelial gaps with sparse underlying meshwork do correlate with plasmin elevation and may facilitate sinusoidal bleeding after APAP overdose.

Fibronection is significantly diminished around hepatic vasculature after APAP overdose

Since excessive plasmin-mediated ECM degradation can compromise embryonic hepatic sinusoidal integrity(5), we immunostained for four major hepatic ECM components following APAP overdose: fibronectin, collagen I, collagen IV, and laminin. At 2 hr after APAP overdose, before we detect significant plasmin elevation (Fig. 2A), we saw no difference in immunostaining for these ECM components compared to saline-treated controls. However, fibronectin, which is abundantly expressed along the sinusoids and can be directly cleaved by plasmin(17), had significantly decreased staining in both centrilobular and periportal regions at 24 hr after APAP overdose (Fig. 4A). Immunoblotting of total liver lysates further confirmed the reduction of fibronectin that occurs by 24hr after APAP overdose (Fig 4B).

Reduction of plasmin rescues APAP-induced perivascular fibronectin degradation

Since plasmin can cleave fibronectin directly or indirectly through activation of matrix metalloproteinases (MMPs), we sought to determine whether APAP-induced fibronectin diminution is plasmin-dependent. We found that fibronectin immunostaining was significantly rescued in TA-treated animals at 24 hr after APAP overdose (Fig. 5A). We also confirmed that TA treatment rescued fibronectin expression in total liver lysates by immunoblotting at 24 hr after APAP overdose (Fig. 5B). Moreover, fibronectin immunostaining (Fig. 5C) and immunoblotting (Fig. 5D) was also rescued in $Plg^{+/-}$ and $Plg^{-/-}$ livers compared to those from WT littermate controls at 24 hr after APAP overdose. Therefore, plasmin reduction rescues perisinusoidal fibronectin as well as sinusoidal bleeding after APAP overdose, which suggests that fibronectin plays an important role in maintaining sinusoidal integrity in the adult liver.

Discussion

Previous studies have reported the ability of plasmin to exacerbate APAP-induced liver injury(11, 12), but the specific and mechanistic contribution of plasmin to APAP-induced hepatic vascular damage has been understudied. We considered this to be a relevant and important question because we recently found that excessive plasmin activity compromises embryonic sinusoidal vascular integrity by promoting hepatic ECM degradation(5). However, we could not predict whether plasmin would cause similar sinusoidal fragility in adult mice, since hepatic ECM composition changes after birth(6). We now report that hepatic plasmin activity is significantly upregulated within 6 hr in a murine APAP overdose model. Moreover, plasmin activity correlates with perisinusoidal fibronectin degradation and bleeding in this model. Therefore, excessive plasmin activity compromises hepatic sinusoidal integrity in both embryos and adult mice, despite the different composition of perisinusoidal ECM before and after birth.

Our TEM analyses at 6 hr after APAP overdose, the time point at which we saw a peak in plasmin activity levels, did not reveal striking morphological abnormalities in centrilobular sinusoidal endothelial cells. Specifically, we did not see evidence of cellular oncosis and vacuolization in sinusoidal endothelial cells, like we did in adjacent hepatocytes. However, we did observe dilated centrilobular sinusoids and an expanded space of Disse in our sections, which is consistent with previous reports(9, 18). Interestingly, these phenotypes were not rescued after pharmacological plasmin inhibition with TA, although TA treatment did reduce perisinusoidal fibronectin degradation and centrilobular sinusoidal bleeding. These data indicate that plasmin does not contribute to sinusoidal dilation or space of Disse expansion after APAP overdose. However, we believe the expanded space of Disse may be responsible for the diffuse fibronectin staining seen in TA-treated mice at 24 hr after APAP overdose (Fig. 5A). Presumably the perisinusoidal fibronectin that is normally degraded by plasmin after APAP overdose can fill the expanded space of Disse when plasmin activity is reduced with TA treatment. Nevertheless, even with this diffuse distribution pattern, the rescue of fibronectin expression still correlates with reduced centrilobular bleeding in TA-treated mice after APAP overdose. Since our SEM data likewise indicate that a meshwork layer reminiscent of ECM is visibly reduced underlying large gaps in sinusoidal endothelial cells after APAP overdose but is rescued after additional TA treatment, we believe that fibronectin-rich ECM presents a physical barrier that impedes red blood cell extravasation.

Our study indicates that fibronectin is reduced around both periportal and centrilobular sinusoids after APAP overdose (Fig. 4A). However, unlike centrilobular sinusoids, periportal sinusoids do not bleed after APAP overdose. The cytochrome P-450 enzyme CYP-4502E1, which metabolizes APAP to its toxic intermediate *N*-acetyl-*p*-benzoquinone imine (NAPQI) that induces cellular damage, is primarily expressed in centrilobular hepatocytes(19). This distribution likely causes the characteristic centrilobular hepatocyte necrosis seen after APAP overdose. Based on the centrilobular sinusoidal bleeding observed after APAP overdose, we believe necrotic hepatocytes contribute to this bleeding, perhaps by compromising the structural support that hepatocytes normally lend to sinusoidal vessels. Nevertheless, our data also indicate that fibronectin restoration after plasmin reduction is sufficient to prevent centrilobular sinusoidal bleeding, even in the presence of necrotic hepatocytes. Therefore, we conclude that fibronectin-rich ECM plays a more critical role than hepatocytes in maintaining centrilobular sinusoidal integrity. However, further studies will be needed to determine whether fibronectin provides important pro-integrity signaling cues to sinusoidal endothelial cells in addition to providing scaffolding and barrier support that maintain sinusoidal integrity.

Despite the fact that reduction of plasmin activity with either pharmacological TA treatment or with genetic plasminogen ablation reduced APAP-induced fibronectin degradation and perisinusoidal bleeding in our study, we did not find that these plasmin inhibition approaches reduced histological evidence of hepatocyte necrosis or serum ALT levels. Our data indicate that plasmin activity and fibronectin degradation do not contribute to APAP-induced hepatocyte damage like NAPQI does. However, these data also stand in contrast to a previous report, in which serum ALT levels and centrilobular necrotic hepatocyte areas were significantly decreased by 24 hr after APAP overdose in mice treated with TA or in $Plg^{-/-}$ mice(11). The cause of this discrepancy at the 24 hr time point is unclear; perhaps it can be

attributed to diet or gut microbiota or the number of times that the respective genetic models were crossed onto the C57Bl/6J background. Nevertheless, we propose that it would be interesting to design future studies investigating whether maintenance of sinusoidal integrity with TA treatment helps to accelerate liver recovery beyond 24 hr after APAP overdose. In light of the report that knockout of the plasminogen activator inhibitor PAI-1 delays liver recovery and regeneration processes after APAP overdose(12), it is reasonable to hypothesize that plasmin-mediated sinusoidal hemorrhage impairs tissue repair in the APAP overdose model. A systematic analysis of the efficacy of TA treatment in preventing sinusoidal bleeding and promoting subsequent tissue repair when administered at varying times after APAP overdose is warranted and could reveal new and therapeutically beneficial options for combating APAP-induced liver damage.

Supplementary Material

Refer to Web version on PubMed Central for supplementary material.

Acknowledgments

We thank Vijay Muthukumar, Shruti Desai, and Jun Xie for assistance with mouse colony maintenance and Griffin lab members for helpful discussions. We also thank Francis Castellino (Notre Dame) for sharing $Plg^{+/-}$ mice and Lisa Whitworth (Oklahoma State University Microscopy Laboratory) for assistance with SEM.

Financial Support: This work was supported by NIH grant P30GM114731 (to C.T.G. and F.L. with Rodger McEver as PI) and by OMRF institutional funds (to C.T.G.).

List of Abbreviations

ALT	alanine aminotransferase
APAP	acetaminophen
ECM	extracellular matrix
MMPs	matrix metalloproteinases
NAPQI	*N*-acetyl-*p*-benzoquinone imine
PAI-1	plasminogen activator inhibitor-1
Plg	plasminogen
qPCR	real-time quantitative PCR
SEM	scanning electron microscopy
TA	tranexamic acid
TEM	transmission electron microscopy
tPA	tissue plasminogen activator
uPA	urokinase plasminogen activator
uPAR	urokinase plasminogen activator receptor

WT wildtype

References

1. Irigoyen JP, Munoz-Canoves P, Montero L, Koziczak M, Nagamine Y. The plasminogen activator system: biology and regulation. Cell Mol Life Sci. 1999; 56:104–132. [PubMed: 11213252]
2. Castellino FJ, Ploplis VA. Structure and function of the plasminogen/plasmin system. Thromb Haemost. 2005; 93:647–654. [PubMed: 15841308]
3. Davis GE, Pintar Allen KA, Salazar R, Maxwell SA. Matrix metalloproteinase-1 and-9 activation by plasmin regulates a novel endothelial cell-mediated mechanism of collagen gel contraction and capillary tube regression in three-dimensional collagen matrices. J Cell Sci. 2001; 114:917–930. [PubMed: 11181175]
4. Ingram KG, Curtis CD, Silasi-Mansat R, Lupu F, Griffin CT. The NuRD chromatin-remodeling enzyme CHD4 promotes embryonic vascular integrity by transcriptionally regulating extracellular matrix proteolysis. PLoS Genet. 2013; 9:e1004031. [PubMed: 24348274]
5. Crosswhite PL, Podsiadlowska JJ, Curtis CD, Gao S, Xia L, Srinivasan RS, Griffin CT. CHD4-regulated plasmin activation impacts lymphovenous hemostasis and hepatic vascular integrity. J Clin Invest. 2016; 126:2254–2266. [PubMed: 27140400]
6. Amenta PS, Harrison D. Expression and potential role of the extracellular matrix in hepatic ontogenesis: a review. Microsc Res Tech. 1997; 39:372–386. [PubMed: 9407547]
7. Yoon E, Babar A, Choudhary M, Kutner M, Pyrsopoulos N. Acetaminophen-Induced Hepatotoxicity: a Comprehensive Update. J Clin Transl Hepatol. 2016; 4:131–142. [PubMed: 27350943]
8. Jaeschke H, Xie Y, McGill MR. Acetaminophen-induced Liver Injury: from Animal Models to Humans. J Clin Transl Hepatol. 2014; 2:153–161. [PubMed: 26355817]
9. Ito Y, Bethea NW, Abril ER, McCuskey RS. Early hepatic microvascular injury in response to acetaminophen toxicity. Microcirculation. 2003; 10:391–400. [PubMed: 14557822]
10. McCuskey RS. The hepatic microvascular system in health and its response to toxicants. Anat Rec (Hoboken). 2008; 291:661–671. [PubMed: 18484612]
11. Sullivan BP, Kassel KM, Jone A, Flick MJ, Luyendyk JP. Fibrin(ogen)-independent role of plasminogen activators in acetaminophen-induced liver injury. Am J Pathol. 2012; 180:2321–2329. [PubMed: 22507835]
12. Bajt ML, Yan HM, Farhood A, Jaeschke H. Plasminogen activator inhibitor-1 limits liver injury and facilitates regeneration after acetaminophen overdose. Toxicol Sci. 2008; 104:419–427. [PubMed: 18469330]
13. Ploplis VA, Carmeliet P, Vazirzadeh S, Van Vlaenderen I, Moons L, Plow EF, Collen D. Effects of disruption of the plasminogen gene on thrombosis, growth, and health in mice. Circulation. 1995; 92:2585–2593. [PubMed: 7586361]
14. Griffin CT, Brennan J, Magnuson T. The chromatin-remodeling enzyme BRG1 plays an essential role in primitive erythropoiesis and vascular development. Development. 2008; 135:493–500. [PubMed: 18094026]
15. Schindelin J, Arganda-Carreras I, Frise E, Kaynig V, Longair M, Pietzsch T, Preibisch S, et al. Fiji: an open-source platform for biological-image analysis. Nat Methods. 2012; 9:676–682. [PubMed: 22743772]
16. Kato H, Adachi N, Ohno Y, Iwanaga S, Takada K, Sakakibara S. New fluorogenic peptide substrates for plasmin. J Biochem. 1980; 88:183–190. [PubMed: 6447693]
17. Martinez-Hernandez A, Amenta PS. The hepatic extracellular matrix. I. Components and distribution in normal liver. Virchows Arch A Pathol Anat Histopathol. 1993; 423:1–11. [PubMed: 8212529]
18. Walker RM, Racz WJ, McElligott TF. Scanning electron microscopic examination of acetaminophen-induced hepatotoxicity and congestion in mice. Am J Pathol. 1983; 113:321–330. [PubMed: 6650662]

19. Anundi I, Lahteenmaki T, Rundgren M, Moldeus P, Lindros KO. Zonation of acetaminophen metabolism and cytochrome P450 2E1-mediated toxicity studied in isolated periportal and perivenous hepatocytes. Biochem Pharmacol. 1993; 45:1251–1259. [PubMed: 8466546]

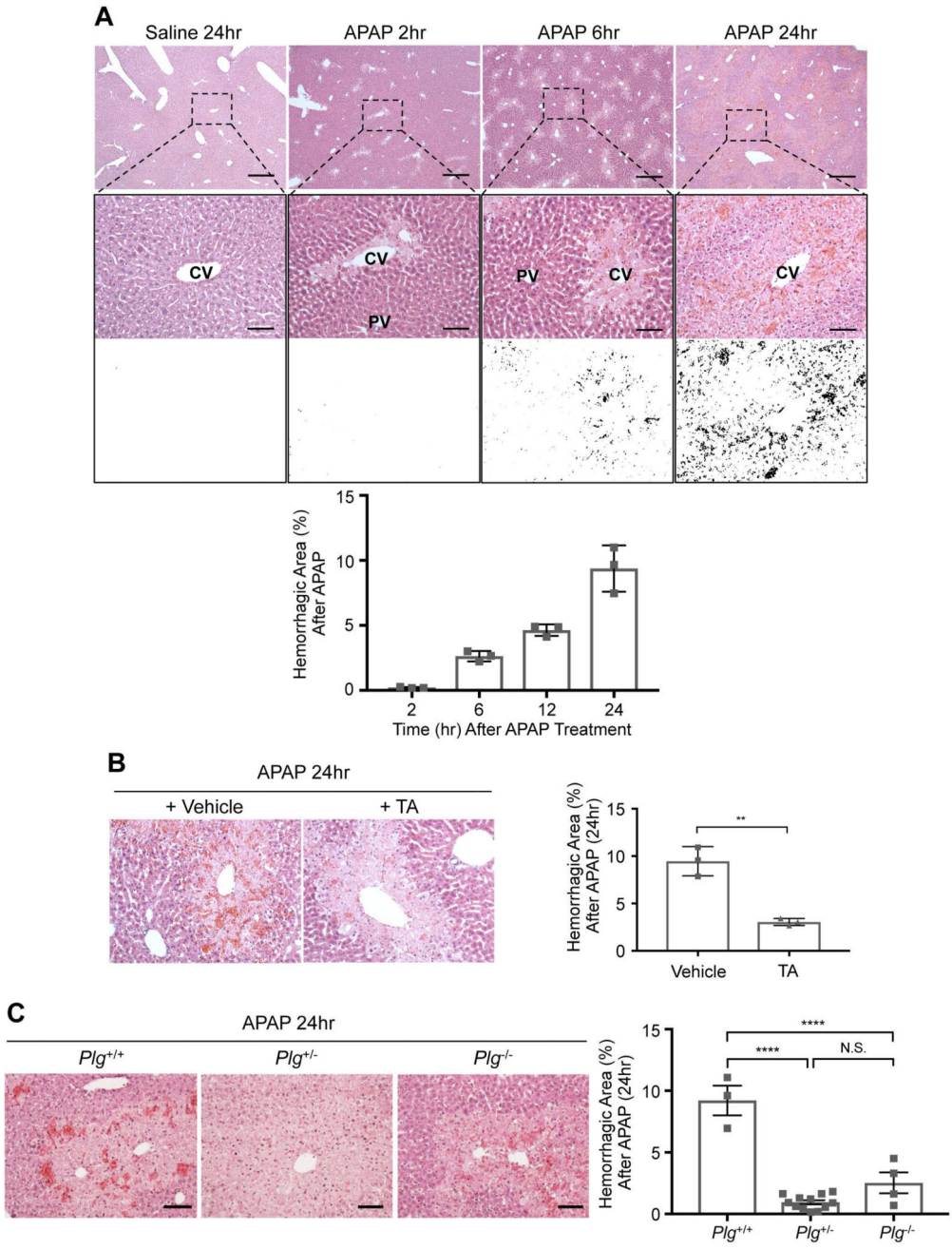

Fig. 1. APAP induced centrilobular sinusoidal bleeding is plasmin dependent

C57Bl/6J male mice were fasted for 16 hr, injected with 300 mg/kg APAP or with saline as a control, and were perfusion fixed and euthanized at indicated times after saline or APAP treatment for histological liver analysis by hematoxylin and eosin staining. (A) Boxed regions of liver sections are magnified below each image and then rendered to black and white contrast images for quantification of the hemorrhagic area (black versus white, as graphed). CV: central vein; PV: portal vein. (B) The pharmacological plasmin inhibitor tranexamic acid (TA; 600 mg/kg) or a vehicle control (saline) was administered 2 hr after APAP overdose, and livers were harvested for analysis at 24 hr after APAP overdose.

Hemorrhagic area was calculated and graphed as in (A). (C) Littermate $Plg^{+/+}$ (WT), $Plg^{+/-}$, and $Plg^{-/-}$ mice were subjected to APAP overdose, and livers were harvested for analysis after 24 hr. Hemorrhagic area was calculated and graphed as in (A). Representative histological images are shown in A-C; each symbol on the graphs represents an average of 5 analyzed sections from an independent animal, and the bars represent the mean hemorrhagic area ± SEM. Statistical analyses were performed using a two-tailed unpaired t-test (B) or a one-way ANOVA with a Tukey's multiple comparisons test (C); $^{**}P<0.01$; $^{****}P<0.0001$. Scale bars: 500 μm (A, upper panel); 100 μm (A, middle panel; B and C).

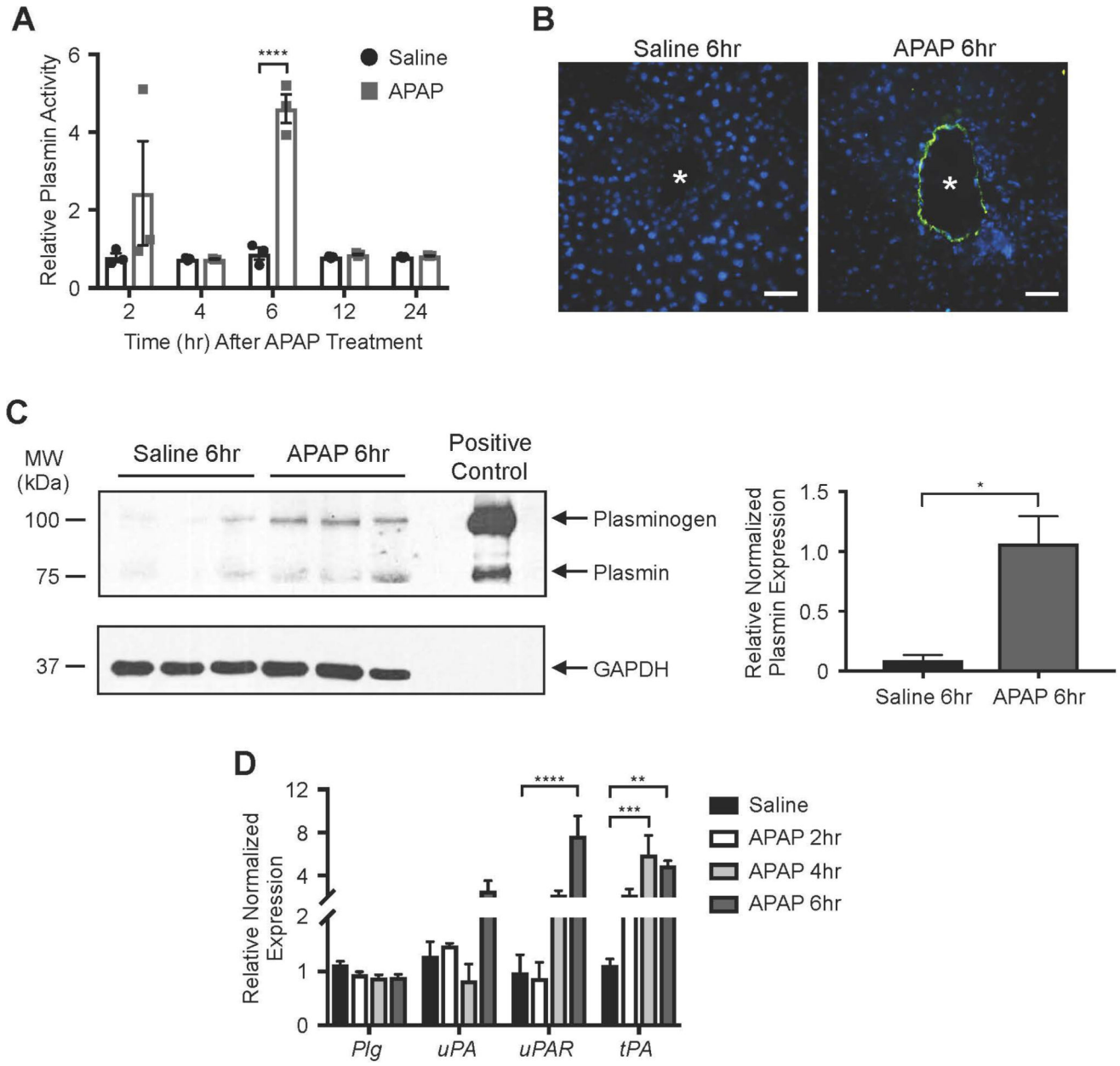

Fig. 2. Plasmin activity is upregulated in murine livers at 6 hr after APAP overdose

(A) Whole liver lysates were generated at specified times after saline versus APAP treatment. Supernatants were used to measure plasmin activity after combination with the plasmin-specific Boc-Glu-Lys-Lys-MCA peptide (10 mmol/L), which fluoresces upon cleavage. Data were generated on a fluorometer and are represented as mean relative plasmin activity ± SEM. (B) Unfixed liver sections collected from mice 6 hr after saline versus APAP treatment were overlaid with Boc-Glu-Lys-Lys-MCA for 30 min at 37°C to detect in situ plasmin activity (green); DAPI (blue) was used as a counterstain. Vessel lumen is marked with an asterisk (*). Images are representative of four independent experiments on sections from different mice. Scale bars: 100 μm. (C) Western blot of plasmin, plasminogen, and GAPDH (loading control) in whole liver lysates collected at 6 hr after saline versus

APAP treatment. Each lane contains a sample from a separate mouse. The positive control lane contains plasminogen from human plasma. Quantification of the individual plasmin bands normalized to respective GAPDH bands and again to the mean APAP treatment value is shown at the right; error bars represent ± SEM. (D) Transcripts for plasminogen (*Plg*), urokinase plasminogen activator (*uPA*), urokinase plasminogen activator receptor (*uPAR*), and tissue plasminogen activator (*tPA*) were measured by qPCR in liver samples collected from mice at the times shown after saline or APAP treatment. Data were normalized to 2 housekeeping control genes and represent mean ± SEM; N=3–4 mice per group. Statistical analyses were performed using a two-way ANOVA with Sidak's multiple comparisons test (A), a two-tailed unpaired t-test (C), or a two-way ANOVA with Dunnett's multiple comparisons test (D); * $P<0.05$; ** $P<0.01$; *** $P<0.001$; **** $P<0.0001$.

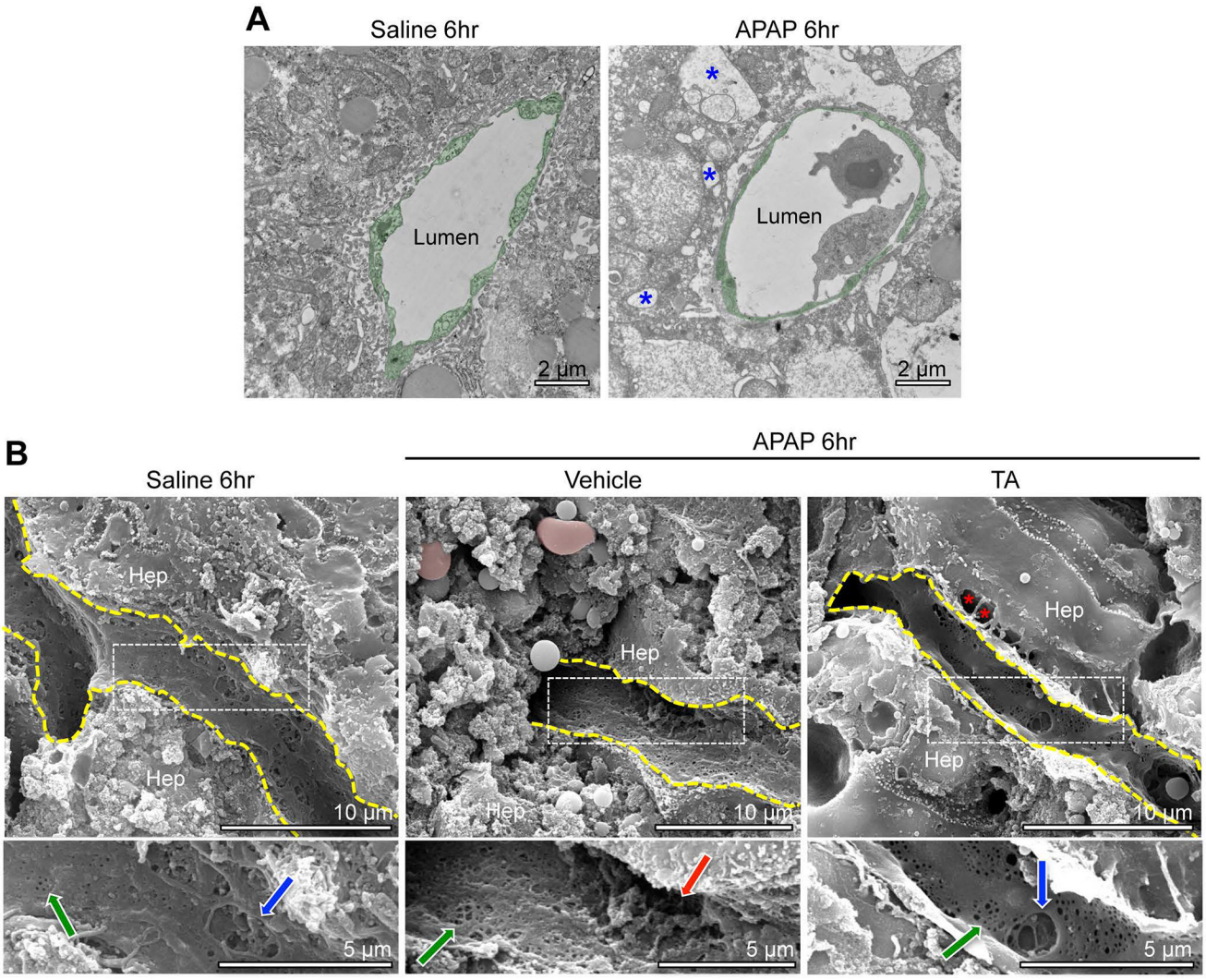

Fig. 3. Sinusoidal endothelial cells do not look necrotic but have cavernous gaps by 6hr after APAP overdose

(A) Two sets of mice treated with saline or APAP for 6 hr were subjected to TEM analysis of centrilobular sinusoidal vessels; representative images are shown. Sinusoidal endothelial cells (artificially pseudocolored in green) show no evidence of swelling and increased vacuolization (blue asterisk), as is seen in surrounding hepatocytes after APAP treatment. (B) Two sets of mice treated with TA or a vehicle control (saline) at 2 hr after APAP overdose were analyzed at 6 hr after APAP overdose and were compared to saline treated animals by SEM. Small fenestrations (green arrows in magnified panels below main images) were seen on the surface of liver sinusoidal endothelial cells (outlined in yellow) under each condition. Larger gaps were likewise seen on the endothelial cell surfaces under each condition, although these gaps appeared to be lined with a fibrous meshwork in samples from saline treated and APAP+TA treated animals (blue arrows in left and right magnified panels). By contrast the larger gaps appeared to be more cavernous and to have less underlying meshwork in samples from APAP+vehicle treated animals (red arrow in center magnified panel). Estravasated red blood cells (pseudocolored in pink) were only detected in

samples from APAP+vehicle treated animals, although an enlarged space of Disse is visible in samples from APAP+TA treated animals (red asterisks). Hep=hepatocyte.

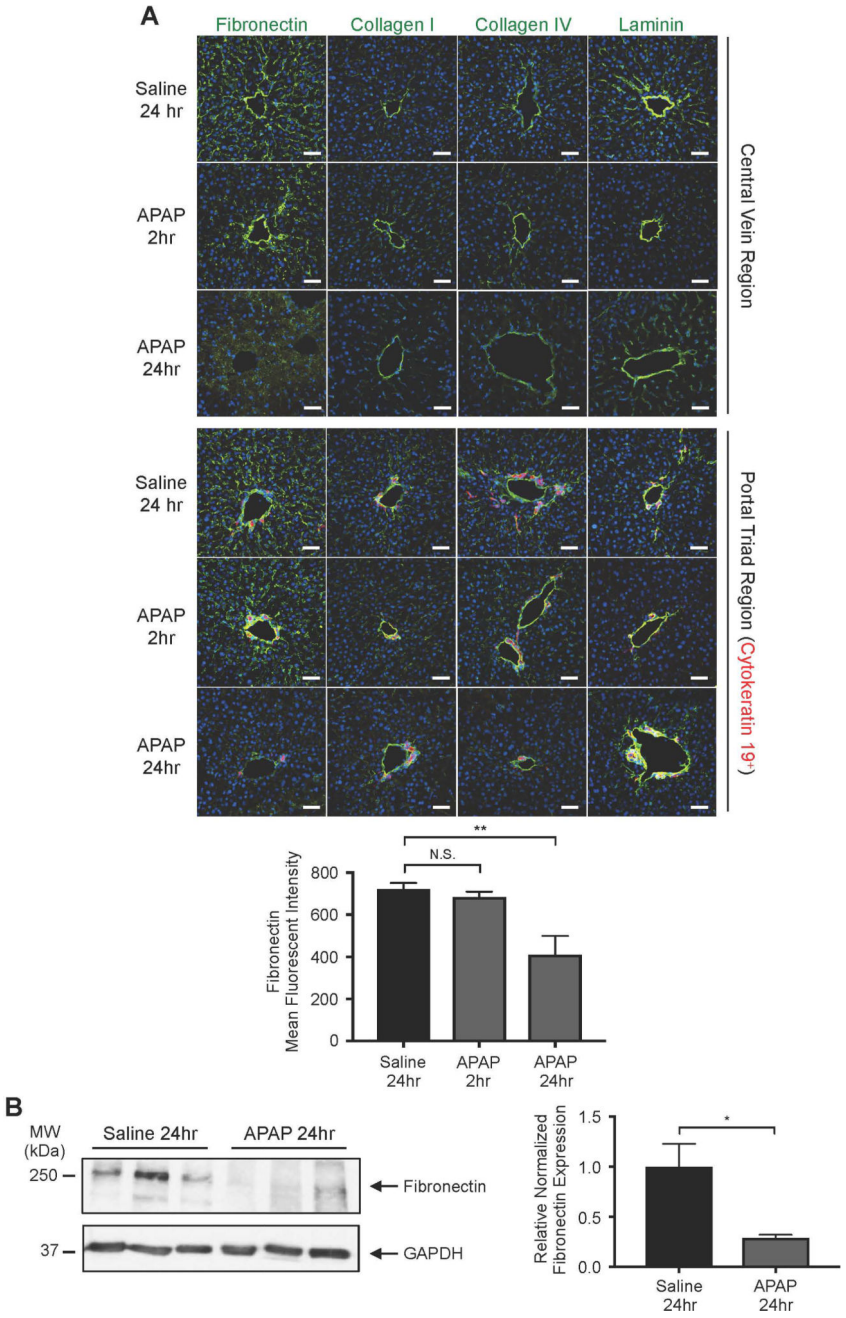

Fig. 4. Fibronectin is significantly degraded around hepatic blood vessels after APAP overdose

(A) The ECM components fibronectin, collagen I, collagen IV, and laminin were each immunostained (green) in liver sections from mice treated with saline for 24 hr or with APAP for 2 or 24 hr. The upper panel depicts immunostaining in the central vein region, while the lower panel depicts staining in the portal triad region, as indicated by the bile duct marker cytokeratin 19 (red). Hoechst (blue) was used as a nuclear counterstain. Scale bars: 50 μm. The graph represents mean fluorescent intensity of fibronectin staining ± SEM, as measured in 4 samples from 3–4 mice. (B) Western blot of fibronectin and GAPDH (loading control) in whole liver lysates collected at 24 hr after saline versus APAP treatment. Each

lane contains a sample from a separate mouse. Quantification of the individual fibronectin bands normalized to respective GAPDH bands and again to the mean saline treatment value is shown at the right; error bars represent ± SEM. Statistical analyses were performed using a one-way ANOVA with Dunnett's multiple comparisons test (A) and an unpaired two-tailed t-test (B); $*P<0.05$; $**P<0.01$.

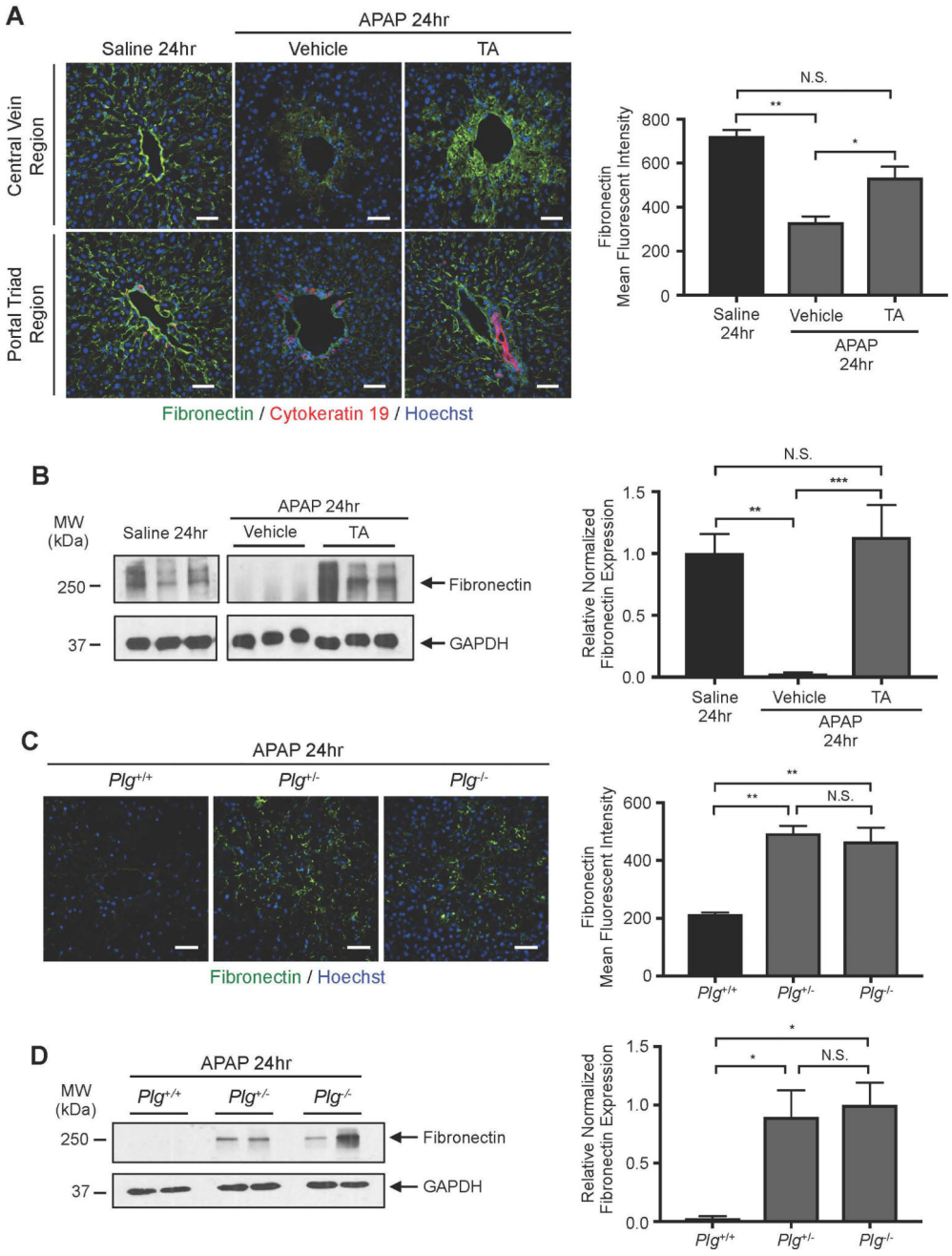

Fig. 5. Plasmin inhibition rescues perisinusoidal fibronectin degradation after APAP overdose

(A) Antibodies against fibronectin (green) and the bile duct marker cytokeratin 19 (red) were used to immunostain liver sections from mice treated with saline or with APAP for 24 hr; Hoechst (blue) was used as a nuclear counterstain. APAP treated animals were also treated with vehicle (saline) or with TA at 2 hr after APAP overdose to assess the impact of pharmacological plasmin inhibition on fibronectin degradation. The graph at right represents mean fluorescent intensity of fibronectin staining ± SEM, as measured in 4 samples from 3–5 mice per group. (B) Western blot of fibronectin and GAPDH (loading control) in whole liver lysates collected at 24 hr after saline versus APAP treatment (+/− TA treatment at 2 hr).

Each lane contains a sample from a separate mouse. Quantification of the individual fibronectin bands normalized to respective GAPDH bands and again to the mean saline treatment value is shown at the right; error bars represent ± SEM. (C) Antibodies against fibronectin (green) were used to immunostain liver sections from littermate $Plg^{+/+}$ (WT), $Plg^{+/-}$, and $Plg^{-/-}$ mice treated with APAP for 24 hr; Hoechst (blue) was used as a nuclear counterstain. The graph at right represents mean fluorescent intensity of fibronectin staining ± SEM, as measured in 4 samples from 3–5 mice per group. (D) Representative western blot of fibronectin and GAPDH (loading control) in whole liver lysates collected at 24 hr after APAP treatment from littermate $Plg^{+/+}$ (WT), $Plg^{+/-}$, and $Plg^{-/-}$ mice. Each lane contains a sample from a separate mouse. Quantification of the individual fibronectin bands normalized to respective GAPDH bands and again to the average value in $Plg^{-/-}$ mice is shown at the right; data represent mean ± SEM from 3–5 mice per group. Statistical analyses for A-D were performed using one-way ANOVA with Bonferroni's multiple comparisons test (A, C), Tukey's multiple comparisons test (B, D); $*P<0.05$; $**P<0.01$; $***P<0.001$. Scale bars: 50 μm.